

Temperature and pressure spikes in ion-beam cancer therapy

Marcel Toulemonde,¹ Eugene Surdutovich,^{2,3} and Andrey V. Solov'yov^{3,*}

¹Laboratory CIMAP-GANIL, CEA-CNRS-ENSICAEN, University of CAEN, Bd. H. Becquerel, 14070 Caen Cedex 5, France

²Department of Physics, Oakland University, Rochester, Michigan 48309, USA

³Frankfurt Institute for Advanced Studies, Ruth-Moufang-Str. 1, 60438 Frankfurt am Main, Germany

(Received 27 May 2009; published 23 September 2009)

The inelastic thermal spike model is applied to liquid water in relation to high-energy $^{12}\text{C}^{6+}$ beams (hundreds of MeV/u) used for cancer therapy. The goal of this project is to calculate the heat transfer in the vicinity of the incident-ion track. Thermal spike calculations indicate a very large temperature increase in the vicinity of ion tracks near the Bragg peak during the time interval from 10^{-15} to 10^{-9} s after the ion's passage and an increase in pressure, as large as tens of MPa, can be induced during that time. These effects suggest a possibility of thermomechanical pathways to disruption of irradiated DNA. An extension of the model for hydrogen, beryllium, argon, krypton, xenon, and uranium ions around the Bragg peak is presented as well.

DOI: [10.1103/PhysRevE.80.031913](https://doi.org/10.1103/PhysRevE.80.031913)

PACS number(s): 87.53.-j, 72.15.Cz, 61.80.-x, 41.75.Ak

I. INTRODUCTION

For more than ten years, heavy-ion-beam cancer therapy has been successfully used clinically in Germany and Japan. Proton-beam therapy is performed in many more centers around the globe and even more facilities are under construction. Thousands of patients per year are being treated. These therapies appear to be a more favorable alternative to the conventional x-ray therapy [1–5].

The therapies have several advantages. Macroscopically, all therapeutic effects are due to the energy loss of ions incident on tissue. The defining feature of ion propagation in tissue is the Bragg peak in the dependence of the linear energy transfer (LET) on the distance along ion tracks. The possibility of tuning the location of the Bragg peak to the tumor depth and the resultant considerable reduction in the dose deposition in the adjacent regions comprise the most important advantage of these therapies.

It is understood that projectiles losing energy due to ionization of a medium produce secondary electrons and radicals (mostly hydroxyl) that cause damage to DNA [6–12]. Some of that damage is irreparable and causes cell death. The type of irreparable damage deemed most important and most often discussed in the literature is double-strand breaking (DSB), which is defined as a break of both strands of DNA on a distance of less than 10 base pairs. One DSB can still be repaired, but if the DSB's are clustered enough, then the damage is lethal.

However, even if clustered DSB's are the predominant cause of cell death, there is still a debate about pathways leading to DSB's. Direct and quasidirect effects [13–16], secondary-electron effects [13,15–17], thermal effects [18], etc. are claimed to be important pathways alone and in relation to each other but are not yet quantified sufficiently. The effects of multiple single-strand breaks (SSBs) coupled with thermal stress and base damage may also comprise a significant fraction of the irreparable damage. The main obstacle to

understanding mechanisms leading to DNA damage is that microscopic events happen on many spatial, temporal, and energetic scales; e.g., time scales for relevant processes vary from 10^{-22} s to minutes. Many thorough papers have been devoted to Monte Carlo (MC) simulations of different fragments of the scenario [19], but they cannot include all scales together and they still do not present a clear picture overall.

All these reasons motivated us to work on a multiscale approach to the physics of ion-beam cancer therapy. In the first series of papers [18,20,21], we addressed the issue of ion propagation and stopping in the medium. In the following works [22,23], we further defined our multiscale approach and tackled the next stage defined by secondary electrons and radicals, which are produced by ionization of molecules of the medium.

However, there is one aspect that has been mentioned in all those papers but has never been thoroughly developed. This is an aspect of heat transfer initiated by the energy loss of projectiles. In this paper, we present the heat transfer during the earliest stage after the ion's passage. The characteristic times of this stage are 10^{-15} – 10^{-9} s. These times are longer than the characteristic time of primary ionization (10^{-15} s) and shorter than typical times of conformational changes in DNA such as unwinding, which are measured in μs or even longer times. Nonetheless, the events, which happen on this intermediate time scale set the initial conditions for the next scales and may be important for the subsequent dynamics of the medium.

In our previous works [18,20,21], we made estimates for the temperature increase in the vicinity of ion tracks. The temperature increase is caused by secondary electrons that acquire most of the energy lost by the stopping ions. Then, this energy is transferred to the medium as electrons become thermalized and bound. The temperature increase strongly depends on the volume within which the energy is deposited. This volume (the cylinder of radii from 3 to 10 nm) has been estimated using the data on the penetration depth of secondary electrons whose average energy is about 45 eV. The maximum average temperature increase was estimated to be about 100°C , which is enough to melt DNA [24]. These estimates have been done for a uniform system in thermal equilibrium, and the energy transport by electrons prior to a

*On leave from A.F. Ioffe Physical Technical Institute, St. Petersburg, Russia.

TABLE I. Thermodynamic parameters for water.

Thermal conductivity ($\text{W K}^{-1} \text{cm}^{-1}$)		6×10^{-3}
Specific heat ($\text{J g}^{-1} \text{K}^{-1}$)	0–273 K	$0.76 \times 10^{-2} T$
	273–373 K	4.18
	>373 K	2
Melting temperature (K)		273
Latent heat of fusion (J g^{-1})		334
Boiling temperature		373
Latent heat of vaporization (J g^{-1})		2257
Density (g cm^{-3})	Solid	0.94
	Liquid	1.0

transfer to the lattice has not been taken into account.

In a number of works, temporal heat transfer in the medium, irradiated by ions, has been studied in relation to quite different applications. In particular, the inelastic thermal spike (i-TS) model has been developed to explain track formation in solids irradiated with heavy ions [25–43]. This model studies the energy deposition to the medium by swift heavy ions through secondary electrons. In this model, the electron-phonon coupling (strength of the energy transfer from electrons to lattice atoms) is an intrinsic property of the irradiated material. Applied to crystalline metals, the i-TS model has been successful in explaining defect annealing at low LET values [31,32,35], damage induced at high LET [32,33,39,40], track formation and sputtering [37,42], and the effect of macroscopic temperature on damage cross section [36]. The electron-phonon coupling agrees with that deduced from electrical resistivity [33] of the considered material.

Irradiated amorphous materials exhibit larger thermal effects than crystalline materials for both metals [35,36,38] and insulators [39,40]. Regarding insulators, a systematic study shows that the damage cross sections can be predicted, assuming an electron-phonon mean free path that decreases monotonically with the band-gap energy [25], following a prediction of Katin *et al.* [41]. Moreover, it is possible to describe the track formation [35,39] (quench of a molten phase) and sputtering (surface evaporation) [37,42] for the

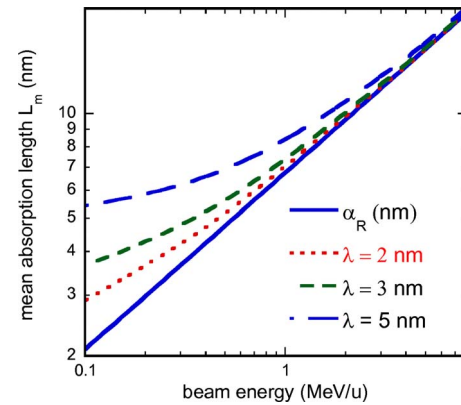


FIG. 1. (Color online) The dependence of the mean absorption length of energy deposition on the beam energy for different values of electron-phonon mean free path, λ . α_r characterizes the radius of a cylinder within which the ion's energy is deposited.

same material or a core shell structure of a track in amorphous SiO_2 [39], as well as the so-called “velocity effect” [26,29,43] in insulators with the same value of the electron-phonon mean free path, which, for the same LET, yields a smaller damage track radius when the ion's velocity is higher.

With this plethora of convergence between experimental results and predictions by the i-TS model, it is appealing to use this model for biological media or liquid water as their substitute because secondary electrons mediate the energy transfer from incident ions to molecular media [44], and studies of amorphous materials suggest that a material such as liquid water with admixtures of amino acids, sugars, etc. is similar to amorphous dielectrics [27,40] and consequently very sensitive to heavy-ion irradiation.

Thermal and pressure spikes in irradiated water were discussed in Ref. [45], where all the energy lost by projectiles was immediately transferred to the lattice thus neglecting the electronic component. As a result, much larger temperature and pressure spikes were predicted even for a smaller LET (the maximum LET considered was 0.4 keV/nm).

In the following sections, we discuss the i-TS model and its application for liquid water and present the results and

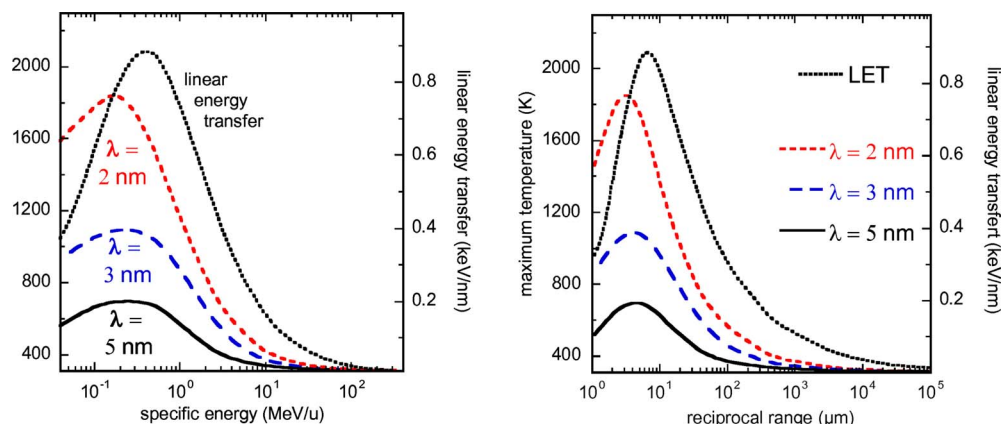


FIG. 2. (Color online) Maximum temperature versus beam energy and reciprocal range for an irradiation with carbon ions for different values of λ . The linear energy transfer (LET) is also plotted in the two pictures.

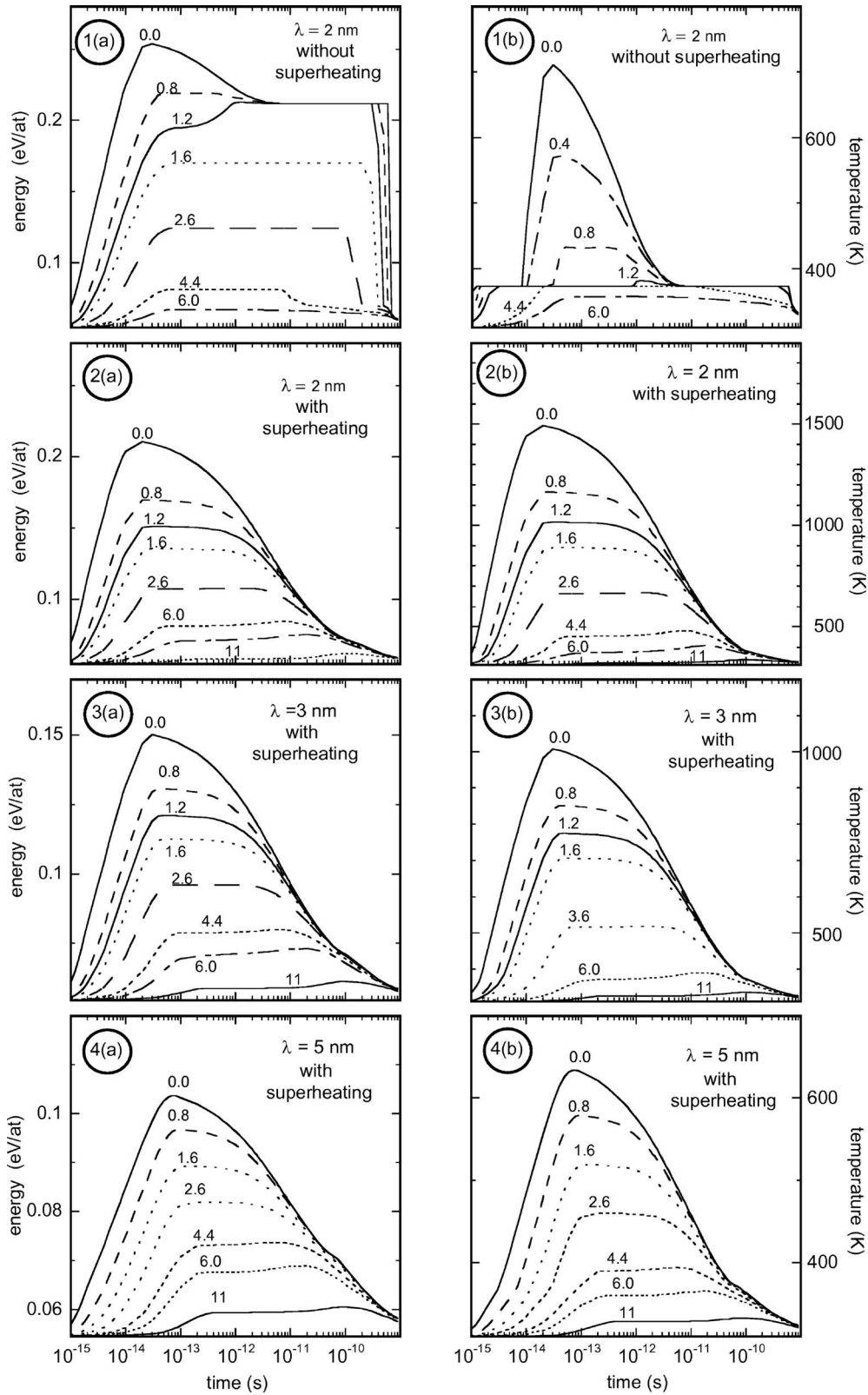


FIG. 3. Energy deposition in eV/atom (the “a” series) and the temperature (the “b” series) on the molecular subsystem versus time for different values of the electron-phonon mean free path [$\lambda=2$ nm for panels 2(a) and 2(b)], [$\lambda=3$ nm for panels 3(a) and 3(b)], [$\lambda=5$ nm for panels 4(a) and 4(b)] assuming a superheating scenario. For the same value of $\lambda=2$ nm, we compare the superheating effect [2(a) and 2(b)] to a nonsuperheating effect [1(a) and 1(b)]. All the calculations have been performed for C ions at 0.5 MeV/u with an electronic energy loss of 0.91 keV/nm [49]. The calculations are carried out for different radii relative to the ion axis. These radii (in nm) are either given near the curve or listed.

their implications regarding the scenario of irradiation of tissue by ions. We use carbon ions as projectiles since they have been used recently in heavy-ion-beam therapies both in Germany and Japan. The calculations are also extended to protons and several different ions around their Bragg peaks. The initial temperature of the medium is taken to be 310 K, the characteristic temperature of a human body.

II. THERMAL SPIKE MODEL FOR LIQUID WATER

The idea of this model is to consider the thermal conductivity by secondary electrons in connection with the lattice thermal conductivity by the medium. These processes are coupled through a quenching energy by electrons interacting with molecules of the medium. The i-TS model mathematically consists of two coupled equations of energy transfer, one into the electron subsystem and the other into the molecular subsystem:

$$C_e \frac{\partial T_e}{\partial t} = \nabla(K_e \nabla T_e) - g(T_e - T) + B[r(\alpha_r), t],$$

$$\rho C(T) \frac{\partial T}{\partial t} = \nabla[K(T) \nabla T] + g(T_e - T), \quad (1)$$

where T_e , T , C_e , C , and K_e , $K(T)$ are the temperatures, specific heats, and thermal conductivities of the electronic and molecular systems, respectively; ρ is the specific mass of the medium and g is an electron-phonon coupling constant. $B[r(\alpha_r), t]$ is the energy density supplied by the incident ion to the electronic system and carried by electrons through a distance r from the ion path deduced from MC calculations [46,47] within a time of the order of $2-3 \times 10^{-15}$ s. The two differential equations are solved numerically using the electron-phonon coupling term, g , as the only parameter [25,29,48]. In contrast to metallic systems, the cooling of the lattice by electron-atom interactions is inhibited when the lattice temperature is larger than the electron temperature [25,29]. This yields the electronic and lattice temperatures, $T_e(t, r)$, $T(t, r)$, around the projectile trajectory as a function of time t and radial distance r .

$B[r(\alpha_r), t]$ is governed by the energy spreading due to collision cascades of electrons. It approximately follows a $1/r^2$ distribution that depends on the ion's velocity and which is approximated using the analytical formula of Wali-gorski [47] deduced from a fit of MC calculations. The radius of a cylinder, α_r , in which 66% of the energy is deposited [29], increases approximately as the square root of the instantaneous beam energy [$\alpha_r(\text{nm}) = 6.8 \times E^{0.51}$] in the case of water, with E ranging between 0.1 and 500 MeV/u. When integrating $B[r(\alpha_r), t]$ over space and time, we assume that the deposited energy is equal to the electronic energy loss as given by SRIM2003 [49]. As previously described [25], the thermodynamic parameters for the electron subsystem take the following values: C_e and K_e are constant throughout the investigated electronic temperature range and equal to $1 \text{ J K}^{-1} \text{ g}^{-1}$ and $2 \text{ W K}^{-1} \text{ cm}^{-1}$, respectively; C and K are deduced from experimental values measured in equilibrium at corresponding lattice temperatures (Table I).

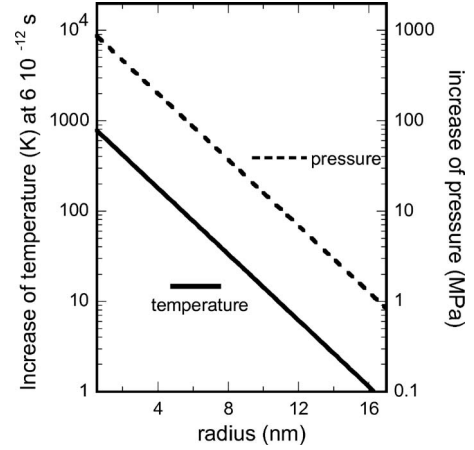


FIG. 4. Increase in temperature (initial value of $T=310$ K) and increase in pressure versus radii in water irradiated by C ions at 0.5 MeV/u with an electronic energy loss of 0.91 keV/nm [49] at a time of 10^{-12} s after the ion passage.

The main parameter in the calculations is the electron-phonon coupling, which is linked to the electron-phonon mean free path, λ , by the relation $\lambda^2 = K_e/g$ [25]. The value of λ defines the diffusion length of the energy carried by electrons prior to its transfer to the lattice; it decreases monotonically with the band-gap energy [48]. The value of λ can be compared to the values of α_r that define the energy spread by electron-collision cascades: the electron-phonon mean free path plays an important role in the energy transfer only if it is larger than α_r . This happens when beam energies are small enough. This is shown in Fig. 1, which displays that the λ plays a significant role for energies less than 3 MeV/u for $\lambda=5$ nm, 1 MeV/u for $\lambda=3$ nm, and 0.5 MeV/u for $\lambda=2$ nm. The mean absorption length of energy deposition on the lattice, L_m , taking into account the electron-phonon mean free path is given by $L_m = \sqrt{\alpha_r^2 + \lambda^2}$. From systematic studies of insulators irradiated by swift heavy ions, it appears that λ depends both on the material and on its structure [25,39,40,42,48]. According to these studies, it has been estimated that λ for water should lie between 1.5–5 nm, similar to solid amorphous materials [27,28,40]. Moreover, an estimate of the electron-mean free path can also be deduced from the work of Voltz [44] who has studied the thermalization of subexcitation electrons in dense molecular media. Such an estimate lies between 1 and 3 nm. Thus, the following several calculations are made with $\lambda=2, 3$, and 5 nm for C ions. More calculations are performed for H, Be, Ar, Kr, Xe, and U ions with an energy loss near the Bragg peak, with $\lambda=2$ nm, the most probable value of the electron-phonon mean free path.

Secondary electrons produced by ions vary in their energies. In principle, the coupling constant g , as well as electron-phonon mean free path λ , may be dependent on the energy of the emerging electron. This dependence, however, is not known even for inorganic materials [25]. Since the electron-phonon mean free path, λ , is larger than the energy deposition length, α , in the energy range below 0.5 MeV/u (Fig. 1), the length, in which the initial electron energy is deposited to the lattice, does not seem to play a significant role.

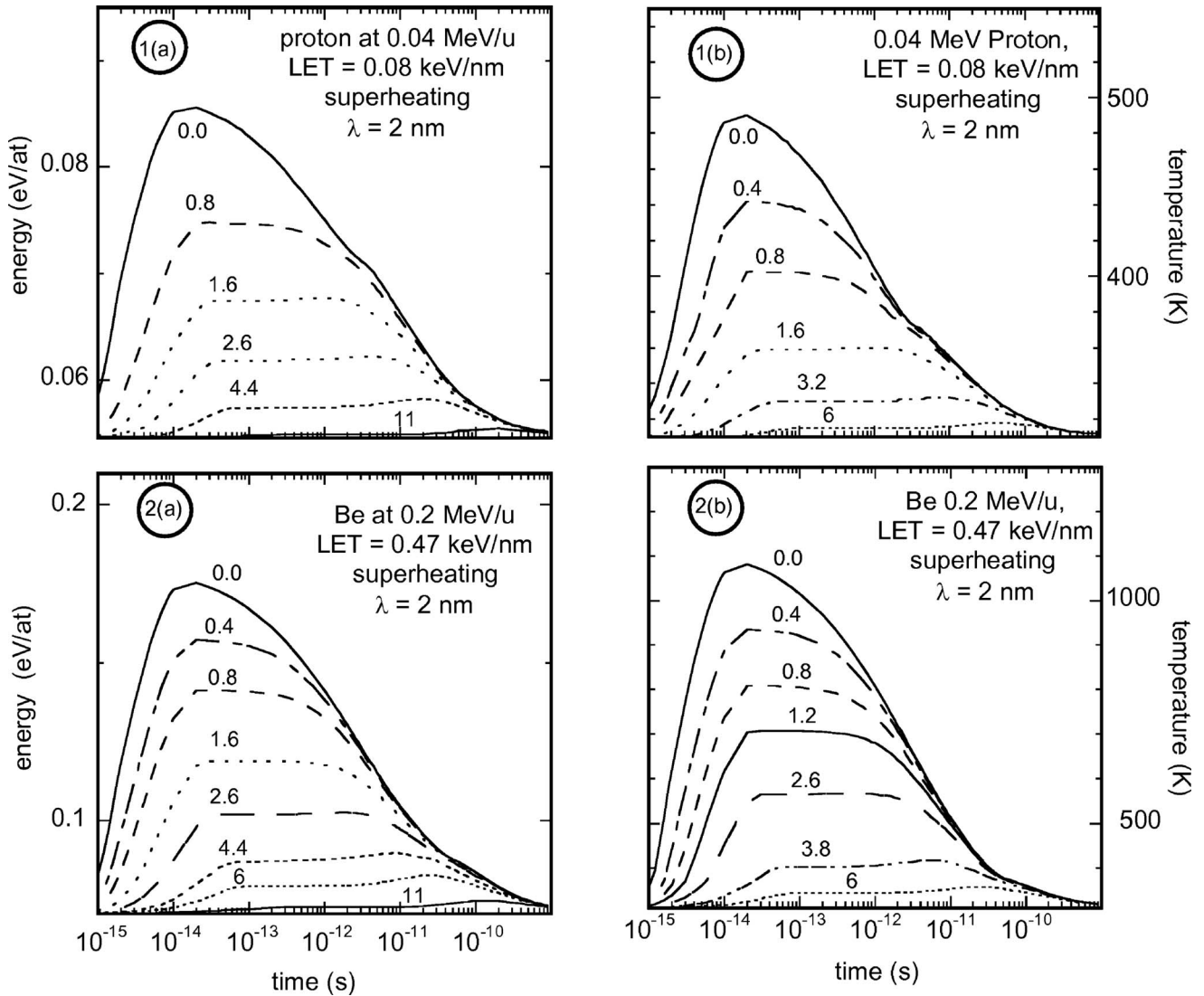


FIG. 5. Energy deposition in eV/atom [panel 1(a)] and the temperature [panel 1(b)] on the lattice subsystem for proton irradiation (0.04 MeV/u with an energy loss of 0.08 keV/nm), assuming a superheating scenario. Same calculations for an intermediate ion, Be [panels 2(a) and 2(b)] at 0.2 MeV/u with an electronic energy loss of 0.47 keV/nm. The calculation is performed for different radii relatively to the ion path. These radii (in nm) are listed.

When computing the temperature profiles around the ion path, the latent heat of a given phase transition is generally taken into account. The method also offers the possibility of considering superheating [50], which takes place when there is rapid heating of the lattice. In this case, the increase in temperature does not stop at the boiling temperature. We shall mainly consider this last scenario since it better describes the sputtering yield and track formation in SiO_2 [42,51] regardless of whether the structure is crystalline or amorphous. However, one example with the latent heat of vaporization is explored for comparison.

III. RESULTS AND DISCUSSION

Figure 2 illustrates the profile of the maximum temperature of water reached during the heat transfer depending on the distance along the track of decelerating 500 MeV/u C

ions. Not surprisingly, the highest temperatures are observed near the Bragg peak, which is about 30 cm deep, has a width of about 1 mm, and where the ion's energy is less than 25 MeV/u. Only there does the temperature increase by more than 30 K. This is true for all considered values of λ and for both scenarios with and without superheating. The figure shows that the maximum temperature may be as large as 1900 K for $\lambda=2$ nm and 700 K for a less probable $\lambda=5$ nm.

This is further substantiated by Fig. 3, which presents series of calculations for C ion in water with $\lambda=2, 3,$ and 5 nm. These results (Fig. 3) present the evolution of the energy per atom (eV/atom) or water temperature versus time for different scenarios for a carbon ion beam of 6 MeV or 0.5 MeV/u (LET=0.91 keV/nm), which corresponds to the energy of carbon ions in the vicinity of the Bragg peak. The first results indicate a sharp increase in temperature for a short time. This increase is much larger than has been previ-

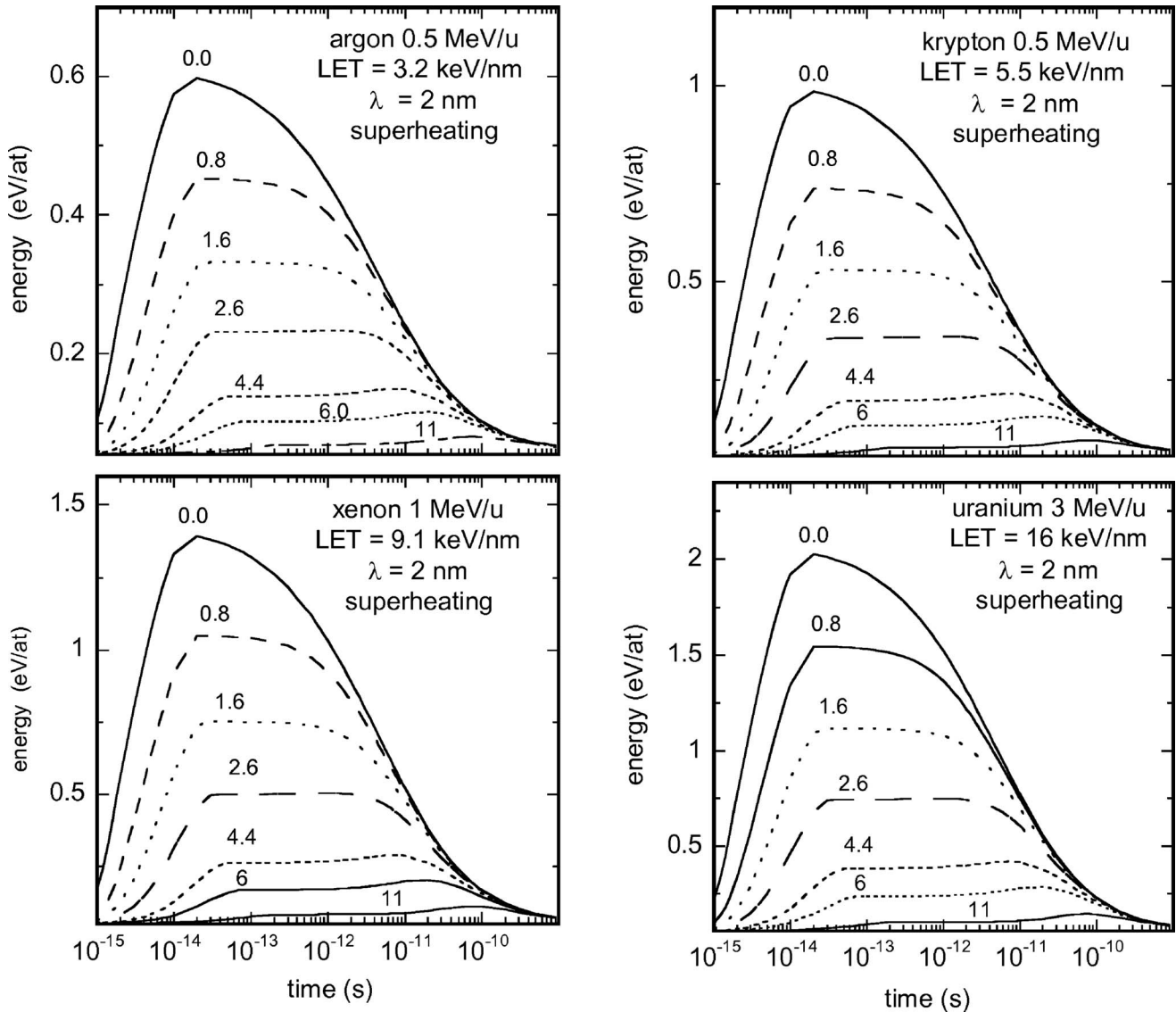


FIG. 6. Energy deposition in eV/atom (left side) on the lattice subsystem for a Ar, Kr, Xe, and U beams with conditions detailed in each picture and assuming a superheating scenario. The calculation is performed for different radii relative to the ion path. These radii (in nm) are listed.

ously estimated in stationary conditions. In the case of $\lambda = 2$ nm, two scenarios are considered in order to confirm that the superheating effect leads to a smaller energy transferred to molecules. During the times between 10^{-15} and 10^{-10} s after the ion's passage, the temperature rises considerably for both scenarios at different distances from the ion track.

In order to interpret these pictures we have to know the thermal energy (in eV/atom) corresponding to the different states of H_2O . At 0 K, the thermal energy is null. Using the evolution of the specific heat of ice versus temperature (Table I), the required energy to reach 310 K is 0.05 eV/atom, taking into account the latent heat of fusion. These two values (310 K and 0.05 eV/atom) are the initial conditions for the calculations. The energy to reach the boiling temperature is 0.065 eV/atom and that to exceed it is 0.21 eV/atom. In the superheating scenario, the equivalent temperatures are 373 and 1495 K, respectively, and the link between the numbers of eV/atom and the temperature is 1.25

$\times 10^{-4}$ eV/atom/K above for T greater than 373 K. The density of liquid water is assumed since in such short times the energy is deposited into superheated liquid water. Notice in Fig. 3 [panels 1(a) and 1(b)], the plateaus are due to latent heat. Figure 3(b) indicates that, regardless of the scenario, the residual temperature increase of 10 K (leading to the temperature of 320 K) is reached within a cylinder of 10 nm radius during 10^{-10} s even when a less probable value of $\lambda = 5$ nm is used. This is in reasonable agreement with our early estimates [18].

An expectation of such a conspicuous effect in water within the i-TS model is based on the above mentioned velocity effect, predicted in insulators as well as in metals [33] with the same value of the electron-phonon mean free path. In relation to this effect, it has been shown [26] that the electronic excitations (largely contributing to $B[r(\alpha_r), t]$ of Eq. (1)) are very important in materials irradiated with low-energy ions. For example, the properties of LiNbO_3 irradi-

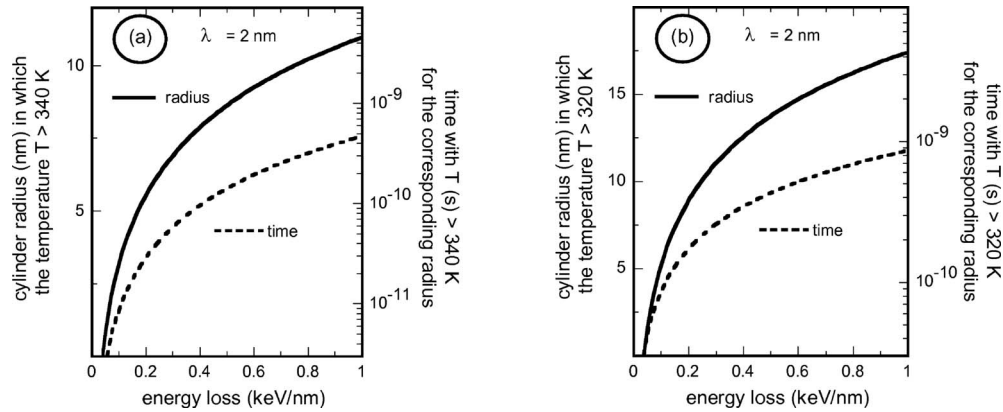


FIG. 7. Using the results of the calculations for H (0.04 MeV), Be (0.2 MeV/u), and C (0.5 MeV/u), the interpolated cylinder radius for lattice temperatures exceeding (a) 340 and (b) 320 K is plotted versus the LET in combination with the time for which the lattice temperature is larger than 340 and 320 K, respectively.

ated with C, N, O, and F ions at ≈ 5 MeV could be associated with damage resulting from the electronic excitations [52]. This result was described *a posteriori* by the i-TS model by Meftah *et al.* [48].

It is interesting to note that for beam energies larger than 100 MeV/u, temperature increase is never more than 10 K. In all cases, the temperature increase is less than 10 K after 10^{-9} s. A minimum pressure increase [53,54] of 11 MPa due to the temperature increase of 10 K is deduced from the coefficient of compressibility (4.5×10^{-10} Pa $^{-1}$) and thermal expansion (5×10^{-4} K $^{-1}$) of water. In a rough estimation, the same parameters are used to calculate the increase in pressure versus radii, shown in Fig. 4, from the temperature reached at a time of 10^{-12} s. These values of pressure give the initial conditions for any hydrodynamics that might follow. From Fig. 4, we can also infer that the pressure gradient in the vicinity (up to 10 nm radius) of the beam is very large, e.g., 25–50 MPa/nm. It provides stresses on DNA molecules, yielding forces of the order of 100 pN or even larger (calculated as pressure drops across or along the characteristic size of 2 nm multiplied by the characteristic area of 4 nm 2). This may well be a separate mechanism for strand breaks. More research is needed to explore this possibility both theoretically and experimentally.

The calculations of thermal spikes were extended to protons, already being used for cancer therapy, as well as for an intermediate ion (Be) between protons and carbon (Fig. 5). The thermal spikes in water irradiated by Ar, Kr, Xe, and U ions at energies around the Bragg peak are plotted in Fig. 6.

Calculations of thermal spikes for different values of LET also allow to study the dependence of the radius of the cylinder within which the temperature increase exceeds a certain value, such as 30 or 10 K. This dependence is shown in Fig. 7; the lifetimes of such temperature increases are reported there as well. Such a calculation provides the information about the regions affected by thermal effects for any ion from proton to carbon and may be important for future calculations on a macroscopic level.

IV. CONCLUSIONS

Our calculations of heat transfer in the vicinity of ion tracks in water using the inelastic thermal spike model pre-

dict very large temperature and pressure increases within 10 nm of the ion trajectories. These spikes may result in considerable forces acting on DNA, which may be large enough to cause mechanical damage, such as strand breaks, and thus be a separate mechanism of DNA damage during irradiation by ions.

Further work, however, is needed to explore, in more detail, how these short-time effects damage DNA. This exploration invites theorists, who should look into DNA dynamics on short time scales (unusual for DNA) as well as experimentalists, who might design an experiment in which thermal effect on DNA could be dominant over effects related to ionization. This work also provides the initial conditions for longer-scale hydrodynamic calculations, which can also be important in the analysis of DNA damage. Such calculations (without taking into account the electronic component) have lead, e.g., to a prediction of ultrasound waves as a result of irradiation with ions [45,55].

Another issue which will have to be addressed is related to chemical changes in the DNA environment and their effects on DNA. It is expected that due to temperature spikes, the rates of chemical reactions increase by orders of magnitude. This concerns the dissociation of water as well as larger molecules. These processes produce more hydroxyl radicals and change the reactivity of the DNA environment. At the same time, DNA itself, which may be partially denaturated, becomes more vulnerable to chemical damage.

Temperature spikes affect the probabilities of direct and quasidirect pathways of DNA damage by means of secondary electrons and holes since the thresholds for some effects (such as vibronic excitation) [14,56,57] are comparable to the energies transferred to the DNA via the heat conductance mechanisms described in this paper. This means that ionization of DNA with its concurrent heating may be the dominant pathway of strand breaks.

E.S. is grateful to J. S. Payson for his critiques and commitment to our research. This work also profited from numerous discussions of E.S. with M. D. Sevilla. We also appreciate the support of Deutsche Forschungsgemeinschaft.

- [1] U. Amaldi and G. Kraft, *J. Radiat. Res. (Tokyo)* **48**, A27 (2007).
- [2] U. Amaldi and G. Kraft, *Rep. Prog. Phys.* **68**, 1861 (2005).
- [3] E. Pedroni, *Europhys. News* **31**, 18 (2000).
- [4] M. Goitein, A. Lomax, and E. Pedroni, *Phys. Today* **55**(9), 45 (2002).
- [5] H. Tsujii *et al.*, *New J. Phys.* **10**, 075009 (2008).
- [6] D. Goodhead, J. Thacker, and R. Cox, *Int. J. Radiat. Biol.* **63**, 543 (1993).
- [7] F. Cucinotta, H. Nikjoo, and D. Goodhead, *Radiat. Environ. Biophys.* **38**, 81 (1999).
- [8] H. Nikjoo, P. O'Neill, M. Terrisol, and D. T. Goodhead, *Radiat. Environ. Biophys.* **38**, 31 (1999).
- [9] J. Cadet, T. Douki, and J. L. Ravanat, *Acc. Chem. Res.* **41**, 1075 (2008).
- [10] J. Kiefer, *Biological Radiation Effects* (Springer-Verlag, Berlin, Heidelberg, New York, 1990).
- [11] R. Kanaar, J. Hoeijmakers, and D. van Gent, *Trends Cell Biol.* **8**, 483 (1998).
- [12] D. Frankenberg, M. Frankenberg-Schwager, D. Blöcher, and R. Harbich, *Radiat. Res.* **88**, 524 (1981).
- [13] D. Becker and M. Sevilla, in *Advances in Radiation Biology*, edited by J. Lett (Academic Press, New York, 1993), Vol. 17, pp. 121–180.
- [14] A. Adhikary, A. Kumar, and M. Sevilla, *Radiat. Res.* **165**, 479 (2006).
- [15] D. Becker, A. Adhikary, and M. Sevilla, *Charged Particle and Photon Interactions with Matter Recent Advances, Applications, and Interfaces* (CRC Press/Taylor & Francis, Boca Raton/London, in press).
- [16] A. Kumar and M. Sevilla, in *Radical and Radical Ion Reactivity in Nucleic Acid Chemistry*, edited by M. Greenberg (Wiley & Sons, New York, 2009).
- [17] L. Sanche, *Eur. Phys. J. D* **35**, 367 (2005).
- [18] E. Surdutovich, O. I. Obolensky, E. Scifoni, I. Pshenichnov, I. Mishustin, A. V. Solov'yov, and W. Greiner, *Eur. Phys. J. D* **51**, 63 (2009).
- [19] H. Nikjoo, S. Uehara, D. Emfietzoglou, and F. A. Cucinotta, *Radiat. Meas.* **41**, 1052 (2006).
- [20] E. Surdutovich, O. Obolensky, I. Pshenichnov, I. Mishustin, A. V. Solov'yov, and W. Greiner, in *Latest Advances in Atomic Cluster Collisions: Structure and Dynamics from the Nuclear to the Biological Scale*, edited by A. Solov'yov and J.-P. Connerade (Imperial College Press, London, 2007), pp. 411–425.
- [21] O. I. Obolensky, E. Surdutovich, I. Pshenichnov, I. Mishustin, A. V. Solov'yov, and W. Greiner, *Nucl. Instrum. Methods Phys. Res. B* **266**, 1623 (2008).
- [22] A. V. Solov'yov, E. Surdutovich, E. Scifoni, I. Mishustin, and W. Greiner, in *Proceedings of the 5th International Conference (RADAM 2008)*, edited by K. Tokesi and B. Sulik (AIP, New York, 2008), Vol. 1080.
- [23] A. V. Solov'yov, E. Surdutovich, E. Scifoni, I. Mishustin, and W. Greiner, *Phys. Rev. E* **79**, 011909 (2009).
- [24] J. SantaLucia, Jr., *Proc. Natl. Acad. Sci. U.S.A.* **95**, 1460 (1998).
- [25] M. Toulemonde, Ch. Dufour, A. Meftah, and E. Paumier, *Nucl. Instrum. Methods Phys. Res. B* **166-167**, 903 (2000).
- [26] M. Toulemonde, C. Trautmann, E. Balanzat, K. Hjort, and A. Weidinger, *Nucl. Instrum. Methods Phys. Res. B* **216**, 1 (2004).
- [27] M. Skupinski, M. Toulemonde, M. Lindeberg, and K. Hjort, *Nucl. Instrum. Methods Phys. Res. B* **240**, 681 (2005).
- [28] F. Pawlak, C. Dufour, A. Laurent, E. Paumier, J. Perrière, J. P. Stoquert, and M. Toulemonde, *Nucl. Instrum. Methods Phys. Res. B* **151**, 140 (1999).
- [29] M. Toulemonde, W. Assmann, C. Dufour, A. Meftah, F. Studer, and C. Trautmann, *Mat. Fys. Medd. K. Dan. Vidensk. Selsk.* **52**, 263 (2006).
- [30] C. Dufour, A. Audourd, F. Beuneu, J. Dural, J. Girard, A. Hairie, M. Levalois, E. Paumier, and M. Toulemonde, *J. Phys.: Condens. Matter* **5**, 4573 (1993).
- [31] Z. Wang, C. Dufour, E. Paumier, and M. Toulemonde, *Nucl. Instrum. Methods Phys. Res. B* **115**, 577 (1996).
- [32] C. Dufour, Z. Wang, E. Paumier, and M. Toulemonde, *Bull. Mater. Sci.* **22**, 671 (1999).
- [33] Z. Wang, C. Dufour, E. Paumier, and M. Toulemonde, *J. Phys.: Condens. Matter* **6**, 6733 (1994); **7**, 2525(E) (1995).
- [34] M. Toulemonde, C. Dufour, and E. Paumier, *Phys. Rev. B* **46**, 14362 (1992).
- [35] H. Dammak, D. Lesueur, A. Dunlop, P. Legrand, and J. Morillo, *Radiat. Eff. Defects Solids* **126**, 111 (1993).
- [36] C. Dufour, F. Beuneu, E. Paumier, and M. Toulemonde, *Europhys. Lett.* **45**, 585 (1999).
- [37] H. D. Mieskes, W. Assmann, F. Grüner, H. Kucal, Z. G. Wang, and M. Toulemonde, *Phys. Rev. B* **67**, 155414 (2003).
- [38] M. Toulemonde, C. Dufour, E. Paumier, and F. Pawlak, *Mater. Res. Soc. Symp. Proc.* **504**, 99 (1998).
- [39] A. Meftah, M. Djebara, N. Khalfaoui, and M. Toulemonde, *Nucl. Instrum. Methods Phys. Res. B* **146**, 431 (1998).
- [40] P. Kluth, C. S. Schnohr, O. H. Pakarinen, F. Djurabekova, D. J. Sprouster, R. Giuliani, M. C. Ridgway, A. P. Byrne, C. Trautmann, D. J. Cookson, K. Nordlund, and M. Toulemonde, *Phys. Rev. Lett.* **101**, 175503 (2008).
- [41] V. Katin, Y. Martinenko, and Y. Yavlinskii, *Sov. Tech. Phys. Lett.* **13**, 276 (1987).
- [42] M. Toulemonde, W. Assmann, C. Trautmann, and F. Grüner, *Phys. Rev. Lett.* **88**, 057602 (2002).
- [43] A. Meftah, F. Brisard, J. M. Costantini, M. Hage-Ali, J. P. Stoquert, F. Studer, and M. Toulemonde, *Phys. Rev. B* **48**, 920 (1993).
- [44] R. Voltz, in *Excess Electrons in Dielectric Media*, edited by C. Ferradini and J. Jay-Gerin (CRC Press, Boca Raton, FL, 1991), p. 71.
- [45] Y. Sun and R. Nath, *Med. Phys.* **20**, 633 (1993).
- [46] B. Gervais and S. Bouffard, *Nucl. Instrum. Methods Phys. Res. B* **88**, 355 (1994).
- [47] M. Waligorski, R. Hamm, and R. Katz, *Nucl. Tracks Radiat. Meas.* **11**, 309 (1986).
- [48] A. Meftah, J. M. Costantini, N. Khalfaoui, S. Boudjadar, J. P. Stoquert, F. Studer, and M. Toulemonde, *Nucl. Instrum. Methods Phys. Res. B* **237**, 563 (2005).
- [49] J. F. Ziegler, *Nucl. Instrum. Methods Phys. Res. B* **219-200**, 1027 (2003).
- [50] P. Hermes, B. Danielzik, N. Fabricius, D. von der Linde, J. Kuhl, Y. Heppner, B. Stritzker, and A. Pospieszczyk, *Appl. Phys. A: Mater. Sci. Process.* **39**, 9 (1986).
- [51] W. Assmann, M. Toulemonde, and C. Trautmann, *Top. Appl.*

- Phys. **110**, 401 (2007).
- [52] G. Bentini, M. Bianconi, L. Corra, M. Chiarini, P. Mazzoldi, C. Sada, N. Argiolas, M. Bazzan, and R. Guzzi, *J. Appl. Phys.* **96**, 242 (2004).
- [53] A. Berthelot, S. Hemon, F. Gourbilleau, C. Dufour, E. Dooryhee, and E. Paumier, *Nucl. Instrum. Methods Phys. Res. B* **146**, 437 (1998).
- [54] C. D'Orléans, J. P. Stoquert, C. Estournès, C. Cerruti, J. J. Grob, J. L. Guille, F. Haas, D. Muller, and M. Richard-Plouet, *Phys. Rev. B* **67**, 220101(R) (2003).
- [55] N. Baily, *Med. Phys.* **19**, 525 (1992).
- [56] A. Kumar and M. Sevilla, *J. Phys. Chem. B* **111**, 5464 (2007).
- [57] A. Kumar and M. Sevilla, *J. Am. Chem. Soc.* **130**, 2130 (2008).